authenticated version is available online at: https://doi.org/10.1007/s11664-018-6421-4

Performance analysis and discussion on the thermoelectric element footprint for PV-TE maximum power generation

Guiqiang Li[1*], Xudong Zhao[1*], Yi Jin[2], Xiao Chen[3], Jie Ji[4], Samson Shittu[1]

[1]*School of Engineering, University of Hull, Hull HU6 7RX, UK*

[2]*Department of Precision Machinery and Precision Instrumentation, University of Science and Technology of China, Hefei, Anhui, China*

[3]*State Key Laboratory of Fire Science, University of Science and Technology of China, 96 Jinzhai Road, Hefei City 230026, China*

[4]*Department of Thermal Science and Energy Engineering, University of Science and Technology of China, 96 Jinzhai Road, Hefei City, 230026, China;*

Abstract

The geometry optimization for thermoelectric element is a valuable way to improve the TE efficiency. The Photovoltaic (PV) and Thermoelectric (TE) have a relatively complex relationship and their individual effects means that the geometrical optimization of the TE alone may not be sufficient for the PV-TE. Thus, the parametric optimisation of the geometry of thermoelectric element footprint for a Photovoltaic-Thermoelectric (PV-TE) is introduced in this paper. A uni-couple TE model was built for the PV-TE using the finite element method (FEM) and temperature dependent thermoelectric material properties. Two types of PV cells are analysed in this paper and the performance of PV-TE with different length of TE elements and footprint areas is

analysed. The outcome showed that no matter what the TE elements length and the footprint areas are, the maximum power output occurs when $A_n/A_p=1$. This finding is useful because it would provide a reference whenever PV-TE optimization is investigated.

Keywords: PV-TE, footprint, uni-couple; geometry, finite element method

*Corresponding authors. E-mail: Guiqiang.Li@ hull.ac.uk (G. Li); Xudong.Zhao@hull.ac.uk (X. Zhao).

1. Introduction

One of the most encouraging renewable energy sources are thermoelectric (TE) devices because they can convert heat flux into electricity directly via the Seebeck effect [1]. Some benefits of thermoelectric devices include; noiseless operation, small weight, no moving parts (this increases the system lifetime), increased reliability and significantly reduced maintenance requirements [2,3].

Generally speaking, the two ways to enhance the performance of TE devices [4] are; improving the thermoelectric material characteristics or optimising the existing thermoelectric devices. Specifically, the optimisation of TE element geometry has been the subject of increased research. Sahin and Yilbas investigated the influence of leg geometry on the performance of thermoelectric device and presented that the shape parameter positively affects the efficiency but negatively affects the power output [5]. Marcin Borcuch et al. presented the influence of fin geometry design, in hot-side heat

exchangers, upon the operational parameters of a thermoelectric generator [6]. Wang et al. presented the design of heat sink geometry including fin spacing and length with two-stage optimisation [7]. Yilbas BS and Ali H introduced the dimensionless tapering parameter and analysed its effect on the first and second law efficiencies on various operating conditions [8].Jang and Tsai optimised Thermoelectric module spacing and spreader thickness using a simplified conjugate-gradient method [9]. Zu-Guo Shen et al. theoretically analysed the performance of annular thermoelectric couple [10]. Ravita Lamba and S.C. Kaushik studied the influence of Thomson effect and leg geometry configuration on the performance of TEG [11]. Haider Ali et al. performed the thermodynamic analysis of a thermoelectric generator considering the geometric configuration of the device pins, and they found the thermal efficiency of the generator can be enhanced by increasing the dimensionless geometric parameter[12]. Lavric performed a 1-dimensional thermal analysis of thermoelectric devices considering the geometry and found that the electrical resistance is reduced by decreasing the leg length of the thermoelectric element. However, longer leg length would result in a greater temperature difference between the two ends of the legs [13]. A. Rezania et al. optimized the footprint ratio of n- type and p-type TE elements, and results showed that when $A_n/A_p<1$, maximum power generation occurs [14].

Combining Photovoltaic (PV) and Thermoelectric (TE) is a good way to take full advantage of the wider solar spectrum to produce the electricity [15]. The PV can absorb part of the incident solar energy to produce electricity directly, then the remaining solar energy can be converted as the thermal energy passes through the TE

to produce more electricity. Yi-Peng Zhou et al developed the multi-physics coupling mathematic model of the PV-TE hybrid system [16]. Khaled Teffah and Youtong Zhang performed both the modelling and experimental research on hybrid PV-TE system for highly concentrated conversion of solar energy [17].

H. Hashim et al. developed a model for optimising the geometry of thermoelectric devices in a hybrid PV/TE system and argued that in practice, there is a "trade-off" between achieving large output power and using reduced thermoelectric material whenever an optimised geometry is desired [18]. The dimension of the Thermoelectric Generator (TEG) in a hybrid system significantly influences the overall power output of the system because it determines the solar cell's operating temperature and the temperature difference across the TEG. Thus the previousconclusion on the TE geometry optimization may not suitable for the PV-TE system. For example, for the TE alone, when the n- type and p-type footprint are dissymmetrical maximum output power is achieved [14], however it is still unknown if this would be applicable to the PV-TE because of the effect of the interaction between the PV and the TE.

Only a few studies have focused on TE geometry optimisation especially in the footprint area to enhance the hybrid PV-TE system performance. In addition, most recent research in PV-TE have been performed using temperature independent thermoelectric materials. However, the thermoelectric material properties such as electrical resistance, thermal conductivity and the Seebeck coefficient are actually dependent on temperature. Thus, the varying thermoelectric material properties with

temperature would result in different electrical voltage and temperature distributions within the system[19].Based on these facts, this paper focuses on optimizing the geometry of the TE footprint area in a PV-TE system. Temperature dependent TEG material properties are considered and FEM was used to simulate the system. This study will act as a valuable reference when the design of PV-TE geometry is undertaken.

2. Model outline

2.1 Description of a photovoltaic-thermoelectric (PV-TE)

The considered PV-TE uni-couple can be seen from Fig. 1. The surface of the PV cell is where solar irradiation is impinged and a significant portion of this solar irradiation is converted to electricity by the photovoltaic effect. The remaining solar energy is converted to thermal energy, which is partially transferred from the PV to the TE while the remaining is lost to the ambient. This process would result in the occurrence of a temperature difference across the TE hot and cold sides and electricity is produced due to the thermoelectric effect.

2.2 FEM model

The equations used to describe the behaviour of the PV-TE in terms of heat transfer and current density are shown below [20].

$$-k\nabla^2 T + Q = \rho C_p \frac{\partial T}{\partial t} \tag{1}$$

$$\nabla \cdot \left(\xi \frac{\partial \vec{\boldsymbol{E}}}{\partial t} + \vec{\boldsymbol{J}} \right) = Q \tag{2}$$

Where k is the thermal conductivity, T is the temperature field, Q is the internal volume heat source, ρ is the density, C_p is the heat capacity at standard condition, t is the time, ξ is the electric permittivity, $\vec{\boldsymbol{E}}$ is the electrical field. $\vec{\boldsymbol{J}}$ is the current density which is produced by both the Joule effect and Seebeck effect. It is shown as below,

$$\vec{\boldsymbol{J}} = \sigma(\vec{\boldsymbol{E}} - S\nabla T) \tag{3}$$

Where σ is the electrical conductivity and S is the Seebeck coefficient.

$\vec{\boldsymbol{E}}$ is the electric field and is obtained from the electric scalar potential V as

$$\vec{\boldsymbol{E}} = -\nabla V \tag{4}$$

The above differential Eq.s (1) and (2) can be transformed into finite element equations by approximation of the following into interpolation functions; unknown physical field variables, temperature T and electric potential V. Temperature and electric potential can be interpolated using the functions below [21],

$$T = [N]\{T_e\} \tag{5}$$

$$V = [N]\{V_e\} \tag{6}$$

Where V_e is the vector of the nodal electrical potential, T_e is the vector of the nodal temperature, and N is the element shape function.

The FEM model is described by the boundary conditions which are applied to the upper surface of the PV cell. The equation for the external heat flux is given as;

$$q_0 = CG\alpha_c A_c - E_{pv} A_c \quad (8)$$

Where $q_0$is the external heat flux. $C$is the concentration ratio of the solar radiation. G is the solar radiation. $\alpha_c$is the absorptivity of PV cell. A_c is the area of the PV. E_{pv} is the power output of the PV cell per meter square, which is given as;

$$E_{pv} = CG\eta_c[1 - \varphi_c(T_c - 298)] \quad (9)$$

Where η_c is the standard PV efficiency at 25 ℃. φ_c is the solar cell temperature coefficient. T_c is the PV temperature.

Due to the difference in temperature present between the upper surface of the PV and the ambient surroundings, the heat convection is given as

$$q_1 = h_{air} A_c (T_{air} - T_c) \quad (10)$$

Where h_{air} is the convective heat transfer coefficient. The surface radiation heat transfer is written as

$$q_2 = \varepsilon\sigma_b (T_{amb}^4 - T_c^4) A_c \quad (11)$$

Where$T_{amb} = 0.0552 T_{air}^{1.5}$. ε is the emissivity of the PV. σ is Stefan-Boltzmann constant.

The last boundary condition is applied at the cold side. The cold side of the system which is at the bottom is placed in ice water to maintain a constant temperature of 273K. The equation for this condition is given as,

$$T_l = 273K \quad (12)$$

The TE uni-couple open circuit voltage and short circuit voltage are given as,

$$v_{oc} = \bar{\alpha}\Delta\mathrm{T} \tag{13}$$

$$I_{sc} = \frac{v_{oc}}{R} \tag{14}$$

The uni-couple average Seebeck coefficient is given as

$$\bar{\alpha} = \frac{1}{T_h - T_l}\int_{T_c}^{T_h}(\alpha_p - \alpha_n)dT \tag{15}$$

The internal resistance of uni-couple can be expressed as

$$R = R_n + R_p = \left[\left(\sigma_n \frac{A_n}{H_n}\right)^{-1} + \left(\sigma_p \frac{A_p}{H_p}\right)^{-1}\right] \tag{16}$$

The output of the TE uni-couple element can be expressed as

$$P_{TE} = \frac{{v_{oc}}^2}{R+R_L} \tag{17}$$

WhereR_L is the load resistance.

The sum of the PV and TEG respective power outputs give the total power output of and it is given as,

$$P = P_{PV} + P_{TE} = E_{PV}A_c + P_{TE} \tag{18}$$

The PV-TE system efficiency is given as below,

$$\eta = \frac{P}{CGA_c} = \frac{E_{PV}A_c + P_{TE}}{CGA_c} \tag{19}$$

3. Simulation procedure and input parameters

To demonstrate the capability of the developed model for optimal PV-TE design, simulation is performed. Two different types of PV cells possessing two different temperature coefficients and series of TEGs with n- and p-type footprint areas are chosen to investigate their effects on the highest power output. The PV details are shown in Table 1 while the temperature dependent TE materials properties of Bi_2Te_3 used in the FEM simulation can be seen from Fig. 2 [22]. The different TE elements length considered are 5mm, 10mm and 15mm. The n-type and p-type footprint total areas considered are 8 mm^2, 12.5 mm^2, 18 mm^2 and 24.5 mm^2.

The software COMSOL is employed to present the FEM model's temperature and electrical fields. Furthermore, accurate meshing of the PV-TE into small tetrahedrons is done. Details of the PV-TE studied are given in Table 2. An assumption that the code side of the TE is maintained constant at a temperature of 273K was used. For each PV-TE, thirteen cases of the TE n-type and p-type area ratios are considered. These details with the n-type and p-type footprint area ratio are shown in Table 3.

4. Results and discussion

The TEG uni-couple module temperature and voltage distributions are obtained by solving the FEM model. Temperature and voltage distributions in the PV-TE uni-couple using Cell_1 at, $A_n/A_p = 4.18,\ h = 5mm,\ A_n + A_p = 18mm^2,$ are shown in Fig. 3.

Compared to the common works on thermoelectricity where the electrical resistivity, Seebeck coefficient and the thermal conductivity are taken as constants, and the electrical voltage and the temperature distributions are all not uniform. The n-type TE element has a lower temperature difference compared to the p-type TE element due to the n-type material higher thermal conductivity. Thus, across the uni-couple, the heat flux would increase as the footprint area of the n-type element increases. Consequently, if only TEG is considered, the n-type element footprint area is needed to decrease the heat flux flowing across the uni-couple and also to get a high temperature difference across the TE. This would lead to more power output production and this has been verified by [11]. However, due to the effects caused by the combination of the PV and TE [23], the high temperature difference may cause a low PV efficiency. Therefore, for a PV-TE, the TE alone optimization result that highest electrical power generation occurs when $A_n/A_p<1$ maybe not suitable.

The maximum PV-TE efficiency using Cell_1 can be seen from Fig. 4. The TE elements lengths considered are 5mm, 10mm and 15mm as shown in Fig. 4(a), Fig. 4(b) and Fig. 4(c) respectively. No matter what the length is, the maximum power outputs all occur when the areas of the n-type and p-type footprint are the same. Also, when the length is constant, no matter what the areas of the TE footprints are, the maximum power outputs all occur when the n-type and p-type footprint area are asymmetric. This implies that the maximum PV-TE power output occurs when $A_n/A_p = 1$.

In addition, Fig. 4(a) shows that the maximum PV-TE efficiency occurs at $A_n + A_p = 8mm^2$ when the TE element length is 5mm. Also, the highest efficiency decreases as the n-type and p-type area sum increase. However, Fig. 4(c) shows that the minimum efficiency occurs at $A_n + A_p = 8mm^2$ when the TE element length is 15mm and it increases as the n-type and p-type area sum increases.

The results show that at $A_n/A_p=1$, the PV-TE has the highest efficiency based on Cell_1. With different uni-couple footprint areas, the values of PV-TE efficiencies corresponding to the length of TE elements have been shown in Fig.5. The highest efficiency with $A_n=A_p=2$ mm^2 is lower than that with a larger footprint area. But with the footprint area increase, the highest PV-TE efficiency occurs at the larger length of TE element and the curve of the efficiency has a tendency to go up and down with the increase of TE element length.

There is a tendency to go up and down for PV-TE efficiency with the same length of TE element when the footprint area increase, as shown in Fig.6. The PV-TE with the short length of TE element has the maximum efficiency with the small footprint area. The long length of TE elements means the one with the larger thermal resistance and electrical resistance, but the larger TE footprint area means the one with the lower thermal resistance and electrical resistance, so the optimal match between the footprint area and the length of TE element can lead to the maximum output.

Considering Cell_2, Fig. 7 shows the relationship between the PV-TE efficiency and different n-type and p-type area ratio. The Cell_2 has a larger temperature coefficient, so the PV-TE has a strict limit that the PV-TE efficiency should be higher than that of PV alone. It is clear that when the length of TE element is 10mm or 15mm, the efficiencies of PV-TE with the total footprint area of 8 mm^2, 12.5 mm2, 18mm^2 and 22.5 mm^2 are all lower than the efficiency of PV alone. But no matter if the PV-TE efficiency is higher or lower, the maximum efficiencies of the PV-TE all occur when the n- type and p- type footprint areas are the same.

Based on Cell_2, when $A_n/A_p=1$, the PV-TE efficiency decreases with the length of TE element decrease, shown in Fig. 8. And when the footprint area is large, the efficiency decline is small with the length of TE element increase. So the PV-TE with the larger footprint area has the advantage because the PV-TE efficiency should be above 15.0 %. As shown in Fig. 9, the curve of PV-TE efficiency increases as the TE footprint area increases. With the same footprint area, a higher efficiency is observed with the short TE element length.

For the TE alone, the small footprint and long length of TE element can lead to the low thermal conductivity and high electrical resistance. Based on $A_n/A_p<1$, considering the economic factor, the geometrical optimisation usually needs to reach the high cost effective. However, for the PV-TE, the total efficiency is not just determined by the TE but also the PV, and the PV and TE can also be affected by each other. The high thermal resistance can enhance the efficiency of TE, however it

weakens the efficiency of PV. Furthermore, the PV has more contribution towards the highest power output of the PV-TE because the its electrical efficiency is high. But different type solar cells have the different characteristics. For Cell_1 with a small temperature coefficient, the high temperature can be reached for TE, so the TE can be optimised in a large geometrical scope, in which the total efficiency can be kept above 15.0%. But for Cell_2 with a large temperature coefficient, the temperature that can enhance the efficiency of TE would reduce the efficiency of PV significantly, and in many cases the PV-TE efficiency is lower than that of the PV. Thus the low temperature can keep a high efficiency of PV but would limit the power output of TE.

The study above has shown that when the n- type and p- type footprint area ratio is symmetric, the PV-TE can achieve its highest efficiency and this is different from that of a TE alone [24]. For the Cell_1, a lot of the PV-TE electrical efficiency are higher than 10% because of the cell's low temperature coefficient. However, the highest efficiency of the PV-TE is still lower than 12.5% no matter the TE elements n-type and p-type length and the area. Looking from an economic perspective, using low values for the length and area of the n- type and p- type TE elements is good for integration with the PV. Furthermore, the economic factor can be considered during the optimisation of the PV-TE employing Cell_2.

5. Conclusions

This study has investigated the optimum footprint area for thermoelectric elements maximum power generation in a PV-TE. Temperature dependent TE material

properties have been considered. Thermoelectricity equations were solved employing the finite element method model. In the uni-couple, temperature and voltage distributions have also been presented.

Results obtained indicated that the PV-TE highest power output occurs when $A_n/A_p=1$ and this is different from that of the TE only in which highest power output occurs when $A_n/A_p<1$. The major contribution to the PV-TE efficiency is from the PV however, temperature has a negative effect on the PV and a positive effect on the TE. Thus, the higher PV performance limits the TE performance on PV-TE. Different n- and p- type areas may increase the temperature difference which would lead to a decrease in the PV-TE efficiency. Therefore, similar n- type and p-type thermoelectric element footprint area has an advantage for PV-TE.

In addition, this study has also shown that the TEG elements length and area in the PV-TE have a different relationship when different solar cells and different temperature coefficients are considered. In summary, the study has demonstrated the maximum PV-TE power generation optimal footprint area ratio and length.

Acknowledgments

The study was sponsored by the Project of EU Marie Curie International Incoming Fellowships Program (745614), National Science Foundation of China (Grant Nos. 51408578, 51611130195), Anhui Provincial Natural Science Foundation (1508085QE96), National Key Research and Development Project (2016YFE0124800), Key Projects of International Cooperation of Chinese Academy

of Sciences (211134KYSB20160005).

References

1. G. Li, J. Ji, G. Zhang, W. He, X. Chen, and H. Chen, *Int. J. Energy Res*. 40, 2117 (2016).
2. G. Li, G. Zhang, W. He, J. Ji, S. Lv, X. Chen, and H. Chen, *Energy Convers. Manag*. 112, 191 (2016).
3. G. Li, W. Feng, Y. Jin, X. Chen, and J. Ji, *Heat Mass Transf*. 53, 3249 (2017).
4. L. E. Bell, *Science*. 321, 1457 (2008).
5. A. Z. Sahin and B. S. Yilbas, *Energy Convers. Manag*. 65, 26 (2013).
6. M. Borcuch, M. Musiał, S. Gumuła, K. Sztekler, and K. Wojciechowski, *Appl. Therm. Eng*. 127, 1355 (2017).
7. C. C. Wang, C. I. Hung, and W. H. Chen, *Energy*. 39, 236 (2012).
8. B. S. Yilbas and H. Ali, *Energy Convers. Manag*. 100, 138 (2015).
9. J. Y. Jang and Y. C. Tsai, *Appl. Therm. Eng*. 51, 677 (2013).
10. Z. G. Shen, S. Y. Wu, and L. Xiao, *Energy Convers. Manag*. 89, 244 (2015).
11. R. Lamba and S. C. Kaushik, *Energy Convers. Manag*. 144, 388 (2017).
12. H. Ali, A. Z. Sahin, and B. S. Yilbas, *Energy Convers. Manag*. 78, 634 (2014).
13. E. D. Lavric, *Energy*21, 133 (2010).
14. A. Rezania, L. A. Rosendahl, and H. Yin, *J. Power Sources*255, 151 (2014).
15. G. Li, X. Zhao, and J. Ji, *Energy Convers. Manag*. 126, 935 (2016).
16. Y. P. Zhou, M. J. Li, W. W. Yang, and Y. L. He, *Appl. Energy*213, 169 (2018).

17. K. Teffah and Y. Zhang, *Sol. Energy*157, 10 (2017).

18. H. Hashim, J. J. Bomphrey, and G. Min, *Renew. Energy*87, 458 (2016).

19. Y. Wang, X. Zhang, L. Shen, N. Bao, C. Wan, N. H. Park, K. Koumoto, and A. Gupta, *J. Power Sources*241, 255 (2013).

20. L.D. Landau, E.M. Lifshitz. *Electrodynamics of continuous media*, 2nd edn. (UK: Butterworth-Heinemann, 1984).

21. T. Seetawan, U. Seetawan, A. Ratchasin, S. Srichai, K. Singsoog, W. Namhongsa, C. Ruttanapun, and S. Siridejachai, *Procedia Eng*. 32, 1006 (2012).

22. A. Heghmanns, M. Beitelschmidt, S. Wilbrecht, K. Geradts, and G. Span, *Mater. Today Proc*. 2, 780 (2015).

23. G. Li, K. Zhou, Z. Song, X. Zhao, and J. Ji, *Energy Convers. Manag*. 161, 155 (2018).

24. G. Li, X. Chen, Y. Jin, and J. Ji, *Energy Procedia*142, 730 (2017).

Figure lists

Table captions

Table1 Parameters of two types of PV cells

Table 2 Parameters used in FEM model

Table 3 Details with the area ratio of n/p TE elements

Nomenclature

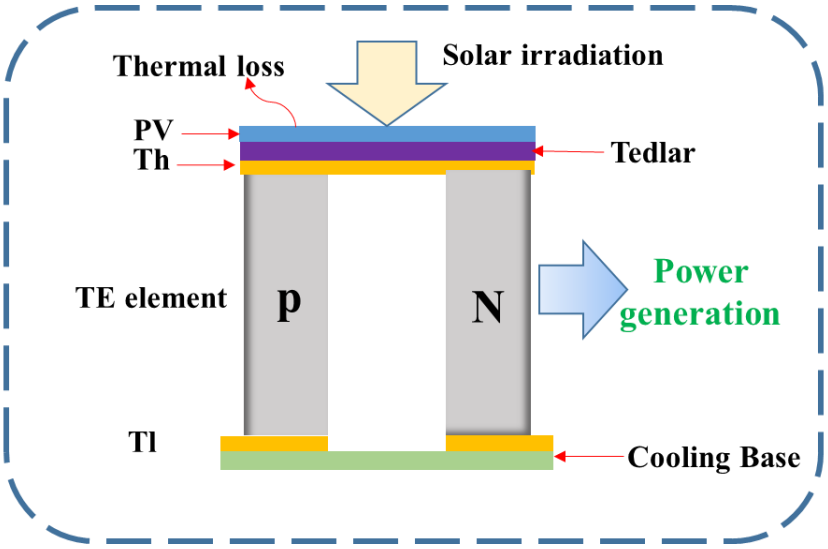

Fig. 1 Schematic diagram of a PV-TE uni-couple

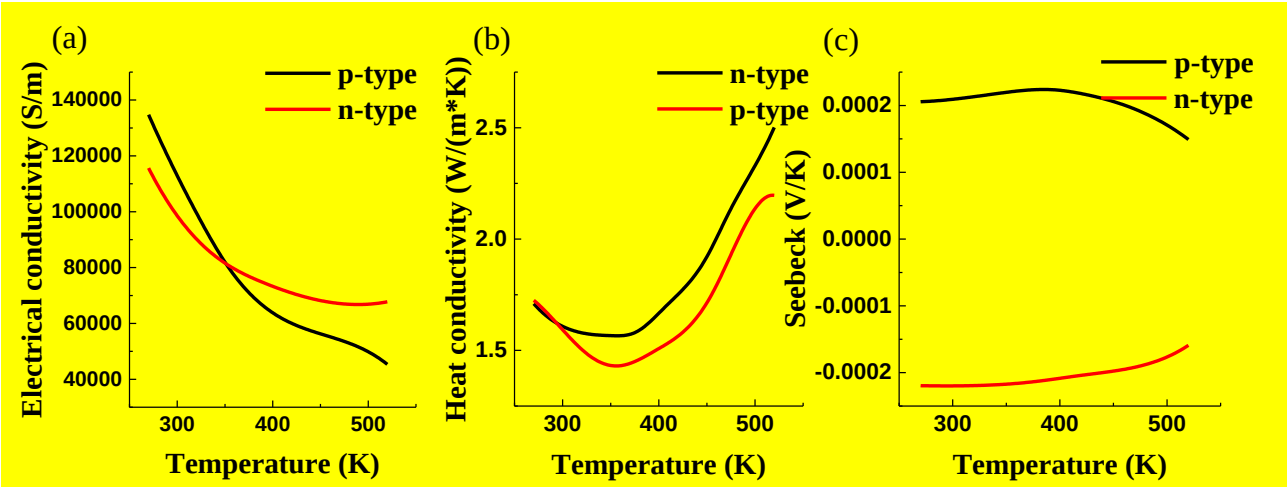

Fig. 2 Properties of the Bi_2Te_3 TE materials (a) Electrical conductivity (b) Heat conductivity (c) Seebeck

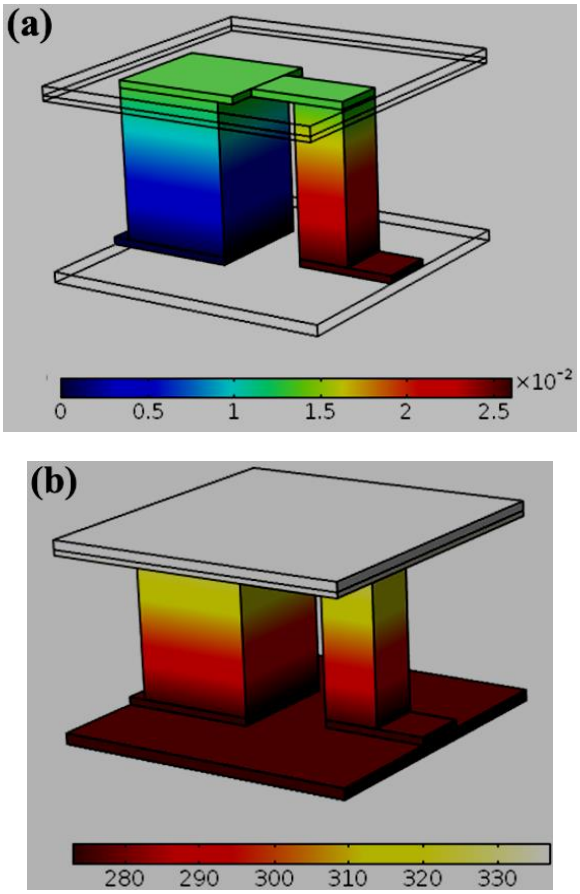

Fig. 3 Schematic diagram (a) generation of the electric voltage, (b) 3D temperature distribution of the PV-TE using PV cell Cell_1, $A_n/A_p = 4.18$, $h = 5mm$, $A_n + A_p = 18mm^2$.

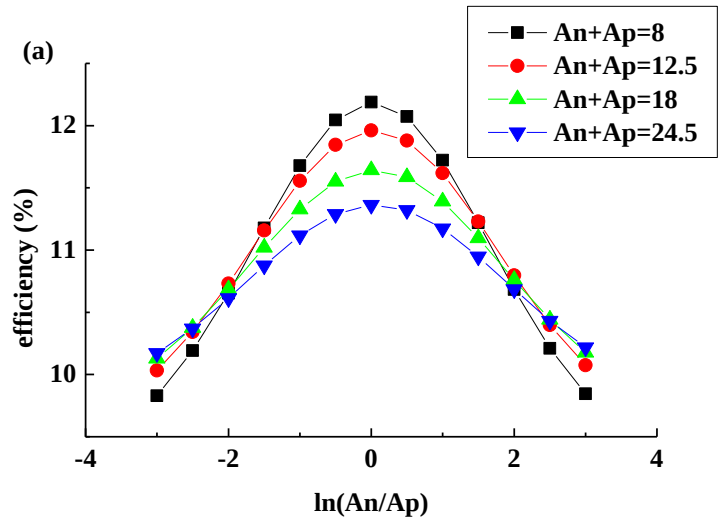
(a)
An+Ap=8
An+Ap=12.5
An+Ap=18
An+Ap=24.5
efficiency (%)
12
11
10
-4
-2
0
2
4
ln(An/Ap)

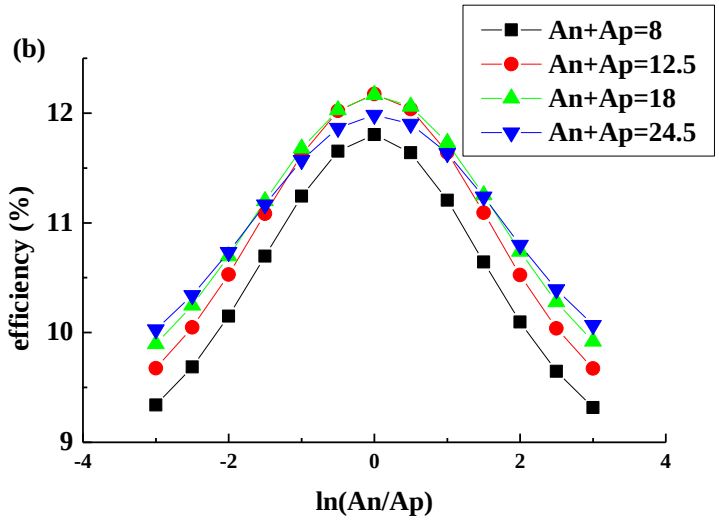
(b)
An+Ap=8
An+Ap=12.5
An+Ap=18
An+Ap=24.5
efficiency (%)
12
11
10
9
-4
-2
0
2
4
ln(An/Ap)

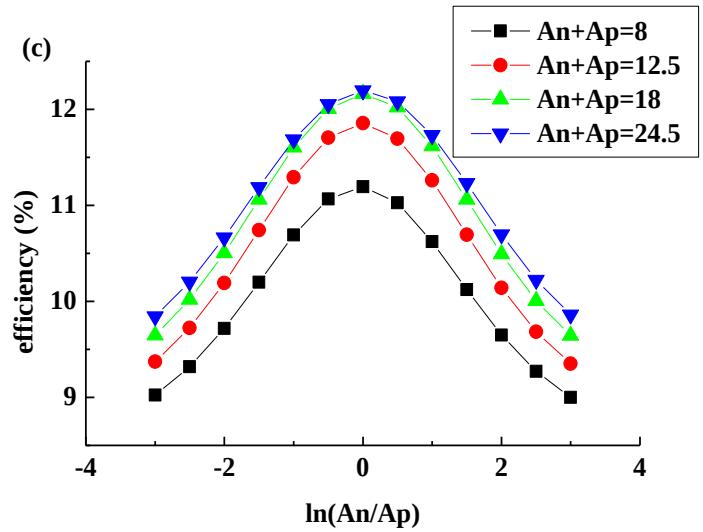
(c)
An+Ap=8
An+Ap=12.5
An+Ap=18
An+Ap=24.5
efficiency (%)
12
11
10
9
-4
-2
0
2
4
ln(An/Ap)

Fig. 4 Variation of the PV/TE efficiency with the area ratio between n-type and p-type using the PV cell Cell_1. The length of TE elements is (a) 5mm, (b) 10mm, (c) 15mm

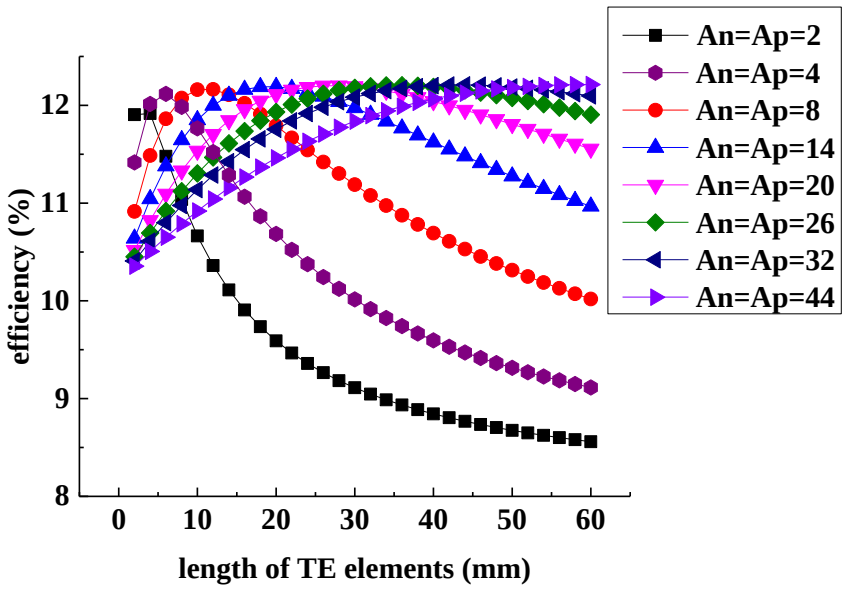

Fig. 5 Variation of the PV-TE efficiency with different length of TE elements based on Cell_1

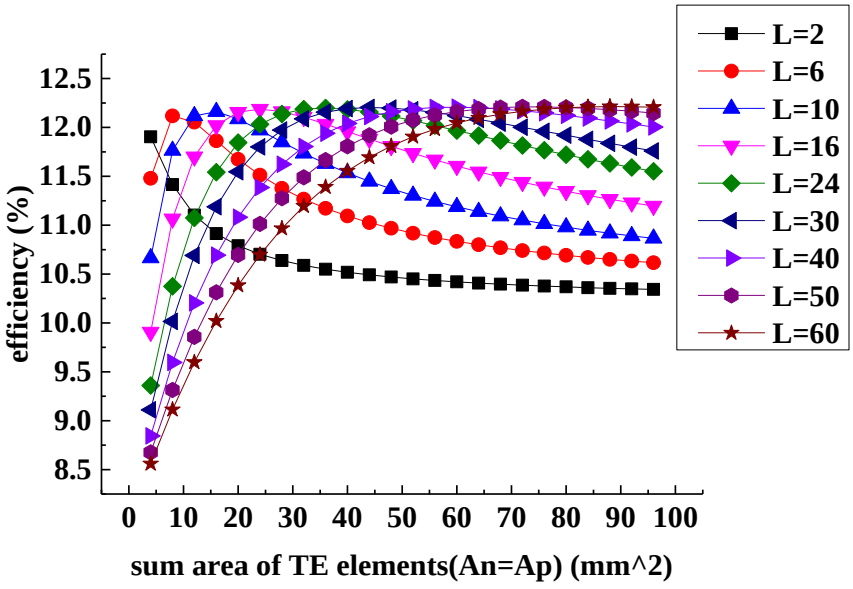

Fig. 6 Variation of the PV-TE efficiency with different footprint areas of TE elements based on Cell_1

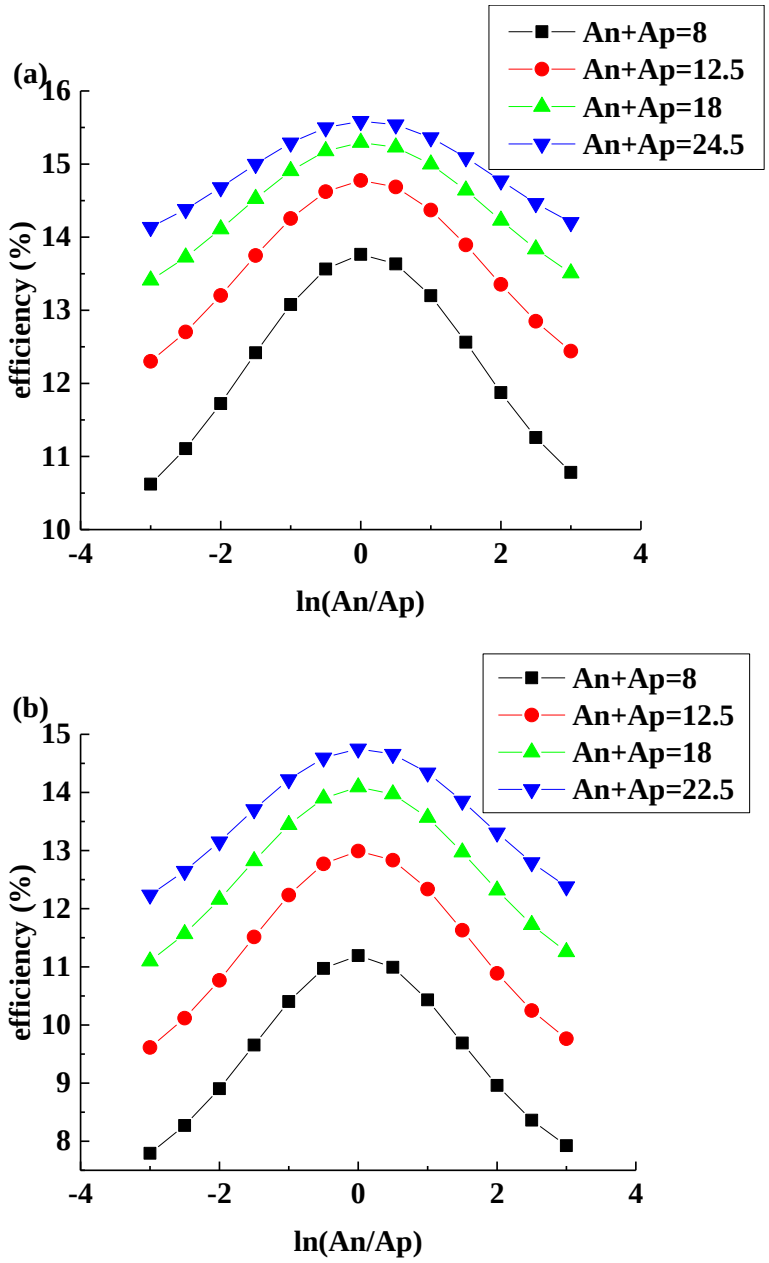

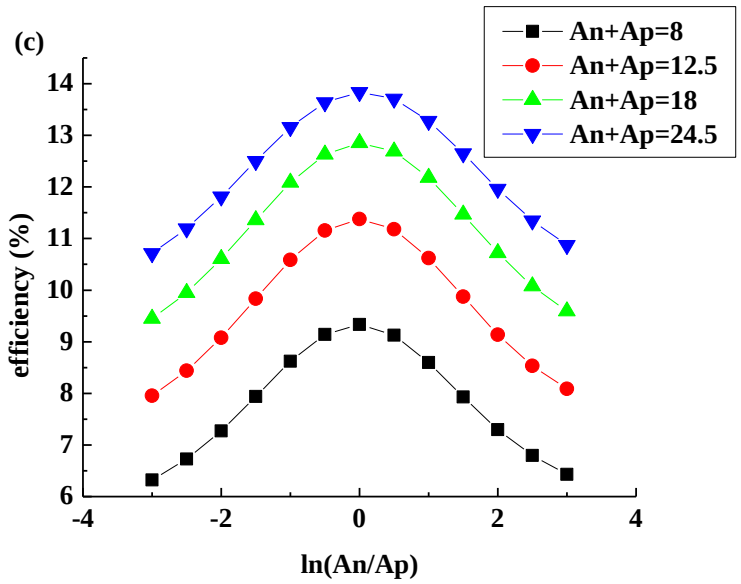

Fig. 7 Variation of the PV/TE efficiency with the area ratio between n-type and p-type using the PV cell Cell_2. The length of TE elements is (a) 5mm, (b) 10mm, (c) 15mm.

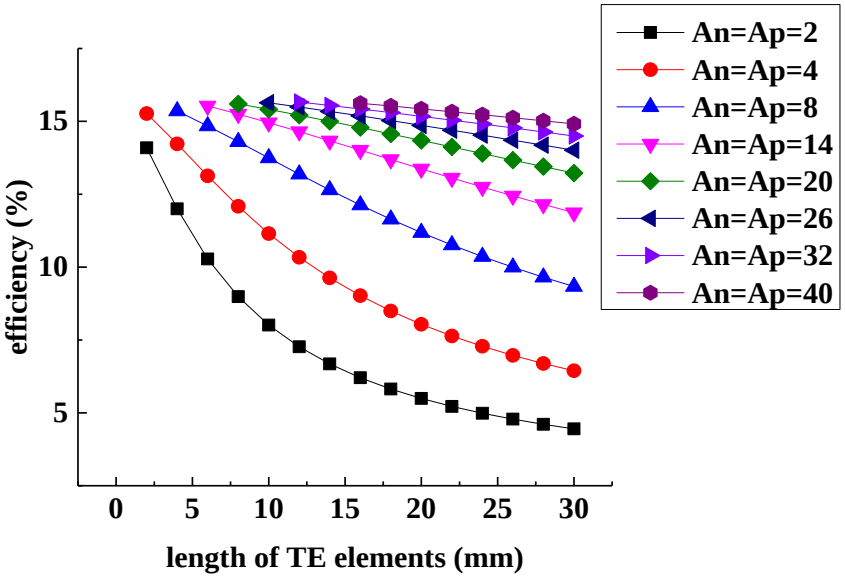

Fig. 8 Variation of the PV-TE efficiency with different length of TE elements based on Cell_2

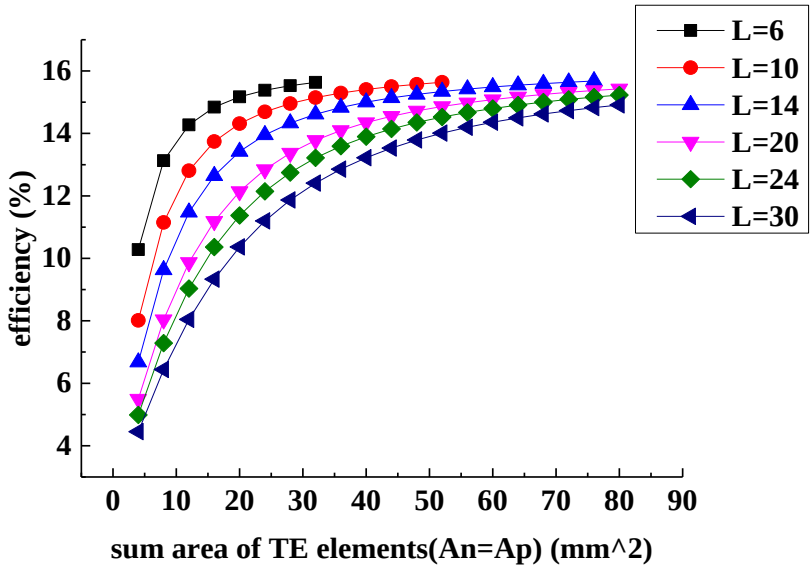

Fig. 9 Variation of the PV-TE efficiency with different footprint areas of TE elements based on Cell_2

Table 1 Parameters used in FEM model

Parameters	Symbol	Value
Area of PV cell	A_c	$10mm \times 10mm$
Thickness of PV cell	H_c	$0.3mm$
Thickness of Tedlar	H_{ted}	$0.175mm$
Thickness of metal sheet	H_{cu}	$0.1mm$
Absorptivity of PV	α_c	0.9
Thermal conductivity of PV	k_c	$148W/(m{\cdot}K)$
Thermal conductivity of tedlar	k_{ted}	$0.2W/(m{\cdot}K)$
Thermal conductivity of metal copper	k_{cu}	$401W/(m{\cdot}K)$
Emissivity of PV	ε	0.8
Ambient temperature	T_{amb}	$298K$
Wind velocity	u_w	$1m/s$
Electrical conductivity of metal copper	μ_{cu}	$58.1 \times 10^6 S/m$
Solar radiation	G	$1000W/m^2$
Concentration ratio	C	5

Table 2 Two types of PV cells used in the study

PV cells	Efficiency at standard condition	Temperature coefficient
Cell_1	10%	$-0.001K^{-1}$
Cell_2	15%	$-0.004K^{-1}$

Table 3 Footprint dimensions of the TE elements with the area ratio of n/p TEG elements

Design NO.	01	02	03	04	05	06	07
A_n / A_p	0.050	0.082	0.135	0.223	0.368	0.607	1.000
Design NO.	08	09	10	11	12	13	
A_n / A_p	1.649	2.718	4.482	7.389	12.182	20.086	

Nomenclature

A_c area of the solar cell (m^2)

A_n area of the n-type of TE element (m^2)

A_p area of the p-type of TE element (m^2)

C concentration ratio

C_p heat capacity at 1 atmosphere ($J \cdot kg^{-1} \cdot K^{-1}$)

E_{PV} power output of the PV cell per square meter($W \cdot m^{-2}$)

G solar irradiance ($W \cdot m^{-2}$)

h convection heat transfer coefficient ($W \cdot m^{-2} \cdot K^{-1}$)

k thermal conductivity ($W \cdot m^{-1} \cdot K^{-1}$)

l_n length of the n-type of TE element (m)

l_p length of the p-type of TE element (m)

P power output of the PV/TE system (W)

P_{PV} electricity generated by PV cell (W)

P_{TE} electricity generated by TEG (W)

T temperature (K)

T_{amb} temperature of the ambient (K)

u_{wind} wind velocity ($m \cdot s^{-1}$)

Greek symbols

α_c absorptivity of PV cell

φ solar cell temperature coefficient(K^{-1})

ρ density ($kg \cdot m^{-3}$)

η efficiency of the PV/TE system

η_c efficiency of the solar cell at standard condition

ε emissivity

σ_b Stefan-Boltzmann's constant ($= 5.67 \times 10^{-8} W \cdot m^{-2} \cdot K^{-4}$)

Performance analysis and discussion on the thermoelectric element footprint for PV-TE maximum power generation

Guiqiang Li[1*], Xudong Zhao[1*], Yi Jin[2], Xiao Chen[3], Jie Ji[4], Samson Shittu[1]

[1]*School of Engineering, University of Hull, Hull HU6 7RX, UK*

[2]*Department of Precision Machinery and Precision Instrumentation, University of Science and Technology of China, Hefei, Anhui, China*

[3]*State Key Laboratory of Fire Science, University of Science and Technology of China, 96 Jinzhai Road, Hefei City 230026, China*

[4]*Department of Thermal Science and Energy Engineering, University of Science and Technology of China, 96 Jinzhai Road, Hefei City, 230026, China;*

Abstract

The geometry optimization for thermoelectric element is a valuable way to improve the TE efficiency. The Photovoltaic (PV) and Thermoelectric (TE) have a relatively complex relationship and their individual effects means that the geometrical optimization of the TE alone may not be sufficient for the PV-TE. Thus, the parametric optimisation of the geometry of thermoelectric element footprint for a Photovoltaic-Thermoelectric (PV-TE) is introduced in this paper. A uni-couple TE model was built for the PV-TE using the finite element method (FEM) and temperature dependent thermoelectric material properties. Two types of PV cells are analysed in this paper and the performance of PV-TE with different length of TE elements and footprint areas is

analysed. The outcome showed that no matter what the TE elements length and the footprint areas are, the maximum power output occurs when $A_n/A_p=1$. This finding is useful because it would provide a reference whenever PV-TE optimization is investigated.

Keywords: PV-TE, footprint, uni-couple; geometry, finite element method

*Corresponding authors. E-mail: Guiqiang.Li@ hull.ac.uk (G. Li); Xudong.Zhao@hull.ac.uk (X. Zhao).

1. Introduction

One of the most encouraging renewable energy sources are thermoelectric (TE) devices because they can convert heat flux into electricity directly via the Seebeck effect [1]. Some benefits of thermoelectric devices include; noiseless operation, small weight, no moving parts (this increases the system lifetime), increased reliability and significantly reduced maintenance requirements [2,3].

Generally speaking, the two ways to enhance the performance of TE devices [4] are; improving the thermoelectric material characteristics or optimising the existing thermoelectric devices. Specifically, the optimisation of TE element geometry has been the subject of increased research. Sahin and Yilbas investigated the influence of leg geometry on the performance of thermoelectric device and presented that the shape parameter positively affects the efficiency but negatively affects the power output [5]. Marcin Borcuch et al. presented the influence of fin geometry design, in hot-side heat

exchangers, upon the operational parameters of a thermoelectric generator [6]. Wang et al. presented the design of heat sink geometry including fin spacing and length with two-stage optimisation [7]. Yilbas BS and Ali H introduced the dimensionless tapering parameter and analysed its effect on the first and second law efficiencies on various operating conditions [8].Jang and Tsai optimised Thermoelectric module spacing and spreader thickness using a simplified conjugate-gradient method [9]. Zu-Guo Shen et al. theoretically analysed the performance of annular thermoelectric couple [10]. Ravita Lamba and S.C. Kaushik studied the influence of Thomson effect and leg geometry configuration on the performance of TEG [11]. Haider Ali et al. performed the thermodynamic analysis of a thermoelectric generator considering the geometric configuration of the device pins, and they found the thermal efficiency of the generator can be enhanced by increasing the dimensionless geometric parameter[12]. Lavric performed a 1-dimensional thermal analysis of thermoelectric devices considering the geometry and found that the electrical resistance is reduced by decreasing the leg length of the thermoelectric element. However, longer leg length would result in a greater temperature difference between the two ends of the legs [13]. A. Rezania et al. optimized the footprint ratio of n- type and p-type TE elements, and results showed that when $A_n/A_p<1$, maximum power generation occurs [14].

Combining Photovoltaic (PV) and Thermoelectric (TE) is a good way to take full advantage of the wider solar spectrum to produce the electricity [15]. The PV can absorb part of the incident solar energy to produce electricity directly, then the remaining solar energy can be converted as the thermal energy passes through the TE

to produce more electricity. Yi-Peng Zhou et al developed the multi-physics coupling mathematic model of the PV-TE hybrid system [16]. Khaled Teffah and Youtong Zhang performed both the modelling and experimental research on hybrid PV-TE system for highly concentrated conversion of solar energy [17].

H. Hashim et al. developed a model for optimising the geometry of thermoelectric devices in a hybrid PV/TE system and argued that in practice, there is a "trade-off" between achieving large output power and using reduced thermoelectric material whenever an optimised geometry is desired [18]. The dimension of the Thermoelectric Generator (TEG) in a hybrid system significantly influences the overall power output of the system because it determines the solar cell's operating temperature and the temperature difference across the TEG. Thus the previousconclusion on the TE geometry optimization may not suitable for the PV-TE system. For example, for the TE alone, when the n- type and p-type footprint are dissymmetrical maximum output power is achieved [14], however it is still unknown if this would be applicable to the PV-TE because of the effect of the interaction between the PV and the TE.

Only a few studies have focused on TE geometry optimisation especially in the footprint area to enhance the hybrid PV-TE system performance. In addition, most recent research in PV-TE have been performed using temperature independent thermoelectric materials. However, the thermoelectric material properties such as electrical resistance, thermal conductivity and the Seebeck coefficient are actually dependent on temperature. Thus, the varying thermoelectric material properties with

temperature would result in different electrical voltage and temperature distributions within the system[19].Based on these facts, this paper focuses on optimizing the geometry of the TE footprint area in a PV-TE system. Temperature dependent TEG material properties are considered and FEM was used to simulate the system. This study will act as a valuable reference when the design of PV-TE geometry is undertaken.

2. Model outline

2.1 Description of a photovoltaic-thermoelectric (PV-TE)

The considered PV-TE uni-couple can be seen from Fig. 1. The surface of the PV cell is where solar irradiation is impinged and a significant portion of this solar irradiation is converted to electricity by the photovoltaic effect. The remaining solar energy is converted to thermal energy, which is partially transferred from the PV to the TE while the remaining is lost to the ambient. This process would result in the occurrence of a temperature difference across the TE hot and cold sides and electricity is produced due to the thermoelectric effect.

2.2 FEM model

The equations used to describe the behaviour of the PV-TE in terms of heat transfer and current density are shown below [20].

$$-k\nabla^2 T + Q = \rho C_p \frac{\partial T}{\partial t} \tag{1}$$

$$\nabla \cdot \left(\xi \frac{\partial \vec{\boldsymbol{E}}}{\partial t} + \vec{\boldsymbol{J}}\right) = Q \tag{2}$$

Where k is the thermal conductivity, T is the temperature field, Q is the internal volume heat source, ρ is the density, C_p is the heat capacity at standard condition, t is the time, ξ is the electric permittivity, $\vec{\boldsymbol{E}}$ is the electrical field. $\vec{\boldsymbol{J}}$ is the current density which is produced by both the Joule effect and Seebeck effect. It is shown as below,

$$\vec{\boldsymbol{J}} = \sigma(\vec{\boldsymbol{E}} - S\nabla T) \tag{3}$$

Where σ is the electrical conductivity and S is the Seebeck coefficient.

$\vec{\boldsymbol{E}}$ is the electric field and is obtained from the electric scalar potential V as

$$\vec{\boldsymbol{E}} = -\nabla V \tag{4}$$

The above differential Eq.s (1) and (2) can be transformed into finite element equations by approximation of the following into interpolation functions; unknown physical field variables, temperature T and electric potential V. Temperature and electric potential can be interpolated using the functions below [21],

$$T = [N]\{T_e\} \tag{5}$$

$$V = [N]\{V_e\} \tag{6}$$

Where V_e is the vector of the nodal electrical potential, T_e is the vector of the nodal temperature, and N is the element shape function.

The FEM model is described by the boundary conditions which are applied to the upper surface of the PV cell. The equation for the external heat flux is given as;

$$q_0 = CG\alpha_c A_c - E_{pv} A_c \quad (8)$$

Where $q_0$is the external heat flux. $C$is the concentration ratio of the solar radiation. G is the solar radiation. $\alpha_c$is the absorptivity of PV cell. A_c is the area of the PV. E_{pv} is the power output of the PV cell per meter square, which is given as;

$$E_{pv} = CG\eta_c[1 - \varphi_c(T_c - 298)] \quad (9)$$

Where η_c is the standard PV efficiency at 25 ℃. φ_c is the solar cell temperature coefficient. T_c is the PV temperature.

Due to the difference in temperature present between the upper surface of the PV and the ambient surroundings, the heat convection is given as

$$q_1 = h_{air} A_c (T_{air} - T_c) \quad (10)$$

Where h_{air} is the convective heat transfer coefficient. The surface radiation heat transfer is written as

$$q_2 = \varepsilon\sigma_b (T_{amb}^4 - T_c^4) A_c \quad (11)$$

Where$T_{amb} = 0.0552 T_{air}^{1.5}$. ε is the emissivity of the PV. σ is Stefan-Boltzmann constant.

The last boundary condition is applied at the cold side. The cold side of the system which is at the bottom is placed in ice water to maintain a constant temperature of 273K. The equation for this condition is given as,

$$T_l = 273K \quad (12)$$

The TE uni-couple open circuit voltage and short circuit voltage are given as,

$$v_{oc} = \bar{\alpha}\Delta\mathrm{T} \tag{13}$$

$$I_{sc} = \frac{v_{oc}}{R} \tag{14}$$

The uni-couple average Seebeck coefficient is given as

$$\bar{\alpha} = \frac{1}{T_h - T_l}\int_{T_c}^{T_h}(\alpha_p - \alpha_n)dT \tag{15}$$

The internal resistance of uni-couple can be expressed as

$$R = R_n + R_p = \left[\left(\sigma_n \frac{A_n}{H_n}\right)^{-1} + \left(\sigma_p \frac{A_p}{H_p}\right)^{-1}\right] \tag{16}$$

The output of the TE uni-couple element can be expressed as

$$P_{TE} = \frac{{v_{oc}}^2}{R+R_L} \tag{17}$$

WhereR_L is the load resistance.

The sum of the PV and TEG respective power outputs give the total power output of and it is given as,

$$P = P_{PV} + P_{TE} = E_{PV}A_c + P_{TE} \tag{18}$$

The PV-TE system efficiency is given as below,

$$\eta = \frac{P}{CGA_c} = \frac{E_{PV}A_c + P_{TE}}{CGA_c} \tag{19}$$

3. Simulation procedure and input parameters

To demonstrate the capability of the developed model for optimal PV-TE design, simulation is performed. Two different types of PV cells possessing two different temperature coefficients and series of TEGs with n- and p-type footprint areas are chosen to investigate their effects on the highest power output. The PV details are shown in Table 1 while the temperature dependent TE materials properties of Bi_2Te_3 used in the FEM simulation can be seen from Fig. 2 [22]. The different TE elements length considered are 5mm, 10mm and 15mm. The n-type and p-type footprint total areas considered are 8 mm^2, 12.5 mm^2, 18 mm^2 and 24.5 mm^2.

The software COMSOL is employed to present the FEM model's temperature and electrical fields. Furthermore, accurate meshing of the PV-TE into small tetrahedrons is done. Details of the PV-TE studied are given in Table 2. An assumption that the code side of the TE is maintained constant at a temperature of 273K was used. For each PV-TE, thirteen cases of the TE n-type and p-type area ratios are considered. These details with the n-type and p-type footprint area ratio are shown in Table 3.

4. Results and discussion

The TEG uni-couple module temperature and voltage distributions are obtained by solving the FEM model. Temperature and voltage distributions in the PV-TE uni-couple using Cell_1 at, $A_n/A_p = 4.18,\ h = 5mm,\ A_n + A_p = 18mm^2,$ are shown in Fig. 3.

Compared to the common works on thermoelectricity where the electrical resistivity, Seebeck coefficient and the thermal conductivity are taken as constants, and the electrical voltage and the temperature distributions are all not uniform. The n-type TE element has a lower temperature difference compared to the p-type TE element due to the n-type material higher thermal conductivity. Thus, across the uni-couple, the heat flux would increase as the footprint area of the n-type element increases. Consequently, if only TEG is considered, the n-type element footprint area is needed to decrease the heat flux flowing across the uni-couple and also to get a high temperature difference across the TE. This would lead to more power output production and this has been verified by [11]. However, due to the effects caused by the combination of the PV and TE [23], the high temperature difference may cause a low PV efficiency. Therefore, for a PV-TE, the TE alone optimization result that highest electrical power generation occurs when $A_n/A_p<1$ maybe not suitable.

The maximum PV-TE efficiency using Cell_1 can be seen from Fig. 4. The TE elements lengths considered are 5mm, 10mm and 15mm as shown in Fig. 4(a), Fig. 4(b) and Fig. 4(c) respectively. No matter what the length is, the maximum power outputs all occur when the areas of the n-type and p-type footprint are the same. Also, when the length is constant, no matter what the areas of the TE footprints are, the maximum power outputs all occur when the n-type and p-type footprint area are asymmetric. This implies that the maximum PV-TE power output occurs when $A_n/A_p = 1$.

In addition, Fig. 4(a) shows that the maximum PV-TE efficiency occurs at $A_n + A_p = 8mm^2$ when the TE element length is 5mm. Also, the highest efficiency decreases as the n-type and p-type area sum increase. However, Fig. 4(c) shows that the minimum efficiency occurs at $A_n + A_p = 8mm^2$ when the TE element length is 15mm and it increases as the n-type and p-type area sum increases.

The results show that at $A_n/A_p=1$, the PV-TE has the highest efficiency based on Cell_1. With different uni-couple footprint areas, the values of PV-TE efficiencies corresponding to the length of TE elements have been shown in Fig.5. The highest efficiency with $A_n=A_p=2$ mm^2 is lower than that with a larger footprint area. But with the footprint area increase, the highest PV-TE efficiency occurs at the larger length of TE element and the curve of the efficiency has a tendency to go up and down with the increase of TE element length.

There is a tendency to go up and down for PV-TE efficiency with the same length of TE element when the footprint area increase, as shown in Fig.6. The PV-TE with the short length of TE element has the maximum efficiency with the small footprint area. The long length of TE elements means the one with the larger thermal resistance and electrical resistance, but the larger TE footprint area means the one with the lower thermal resistance and electrical resistance, so the optimal match between the footprint area and the length of TE element can lead to the maximum output.

Considering Cell_2, Fig. 7 shows the relationship between the PV-TE efficiency and different n-type and p-type area ratio. The Cell_2 has a larger temperature coefficient, so the PV-TE has a strict limit that the PV-TE efficiency should be higher than that of PV alone. It is clear that when the length of TE element is 10mm or 15mm, the efficiencies of PV-TE with the total footprint area of 8 mm^2, 12.5 mm2, 18mm^2 and 22.5 mm^2 are all lower than the efficiency of PV alone. But no matter if the PV-TE efficiency is higher or lower, the maximum efficiencies of the PV-TE all occur when the n- type and p- type footprint areas are the same.

Based on Cell_2, when $A_n/A_p=1$, the PV-TE efficiency decreases with the length of TE element decrease, shown in Fig. 8. And when the footprint area is large, the efficiency decline is small with the length of TE element increase. So the PV-TE with the larger footprint area has the advantage because the PV-TE efficiency should be above 15.0 %. As shown in Fig. 9, the curve of PV-TE efficiency increases as the TE footprint area increases. With the same footprint area, a higher efficiency is observed with the short TE element length.

For the TE alone, the small footprint and long length of TE element can lead to the low thermal conductivity and high electrical resistance. Based on $A_n/A_p<1$, considering the economic factor, the geometrical optimisation usually needs to reach the high cost effective. However, for the PV-TE, the total efficiency is not just determined by the TE but also the PV, and the PV and TE can also be affected by each other. The high thermal resistance can enhance the efficiency of TE, however it

weakens the efficiency of PV. Furthermore, the PV has more contribution towards the highest power output of the PV-TE because the its electrical efficiency is high. But different type solar cells have the different characteristics. For Cell_1 with a small temperature coefficient, the high temperature can be reached for TE, so the TE can be optimised in a large geometrical scope, in which the total efficiency can be kept above 15.0%. But for Cell_2 with a large temperature coefficient, the temperature that can enhance the efficiency of TE would reduce the efficiency of PV significantly, and in many cases the PV-TE efficiency is lower than that of the PV. Thus the low temperature can keep a high efficiency of PV but would limit the power output of TE.

The study above has shown that when the n- type and p- type footprint area ratio is symmetric, the PV-TE can achieve its highest efficiency and this is different from that of a TE alone [24]. For the Cell_1, a lot of the PV-TE electrical efficiency are higher than 10% because of the cell's low temperature coefficient. However, the highest efficiency of the PV-TE is still lower than 12.5% no matter the TE elements n-type and p-type length and the area. Looking from an economic perspective, using low values for the length and area of the n- type and p- type TE elements is good for integration with the PV. Furthermore, the economic factor can be considered during the optimisation of the PV-TE employing Cell_2.

5. Conclusions

This study has investigated the optimum footprint area for thermoelectric elements maximum power generation in a PV-TE. Temperature dependent TE material

properties have been considered. Thermoelectricity equations were solved employing the finite element method model. In the uni-couple, temperature and voltage distributions have also been presented.

Results obtained indicated that the PV-TE highest power output occurs when $A_n/A_p=1$ and this is different from that of the TE only in which highest power output occurs when $A_n/A_p<1$. The major contribution to the PV-TE efficiency is from the PV however, temperature has a negative effect on the PV and a positive effect on the TE. Thus, the higher PV performance limits the TE performance on PV-TE. Different n- and p- type areas may increase the temperature difference which would lead to a decrease in the PV-TE efficiency. Therefore, similar n- type and p-type thermoelectric element footprint area has an advantage for PV-TE.

In addition, this study has also shown that the TEG elements length and area in the PV-TE have a different relationship when different solar cells and different temperature coefficients are considered. In summary, the study has demonstrated the maximum PV-TE power generation optimal footprint area ratio and length.

Acknowledgments

The study was sponsored by the Project of EU Marie Curie International Incoming Fellowships Program (745614), National Science Foundation of China (Grant Nos. 51408578, 51611130195), Anhui Provincial Natural Science Foundation (1508085QE96), National Key Research and Development Project (2016YFE0124800), Key Projects of International Cooperation of Chinese Academy

of Sciences (211134KYSB20160005).

References

1. G. Li, J. Ji, G. Zhang, W. He, X. Chen, and H. Chen, *Int. J. Energy Res*. 40, 2117 (2016).
2. G. Li, G. Zhang, W. He, J. Ji, S. Lv, X. Chen, and H. Chen, *Energy Convers. Manag*. 112, 191 (2016).
3. G. Li, W. Feng, Y. Jin, X. Chen, and J. Ji, *Heat Mass Transf*. 53, 3249 (2017).
4. L. E. Bell, *Science*. 321, 1457 (2008).
5. A. Z. Sahin and B. S. Yilbas, *Energy Convers. Manag*. 65, 26 (2013).
6. M. Borcuch, M. Musiał, S. Gumuła, K. Sztekler, and K. Wojciechowski, *Appl. Therm. Eng*. 127, 1355 (2017).
7. C. C. Wang, C. I. Hung, and W. H. Chen, *Energy*. 39, 236 (2012).
8. B. S. Yilbas and H. Ali, *Energy Convers. Manag*. 100, 138 (2015).
9. J. Y. Jang and Y. C. Tsai, *Appl. Therm. Eng*. 51, 677 (2013).
10. Z. G. Shen, S. Y. Wu, and L. Xiao, *Energy Convers. Manag*. 89, 244 (2015).
11. R. Lamba and S. C. Kaushik, *Energy Convers. Manag*. 144, 388 (2017).
12. H. Ali, A. Z. Sahin, and B. S. Yilbas, *Energy Convers. Manag*. 78, 634 (2014).
13. E. D. Lavric, *Energy*21, 133 (2010).
14. A. Rezania, L. A. Rosendahl, and H. Yin, *J. Power Sources*255, 151 (2014).
15. G. Li, X. Zhao, and J. Ji, *Energy Convers. Manag*. 126, 935 (2016).
16. Y. P. Zhou, M. J. Li, W. W. Yang, and Y. L. He, *Appl. Energy*213, 169 (2018).

17. K. Teffah and Y. Zhang, *Sol. Energy*157, 10 (2017).

18. H. Hashim, J. J. Bomphrey, and G. Min, *Renew. Energy*87, 458 (2016).

19. Y. Wang, X. Zhang, L. Shen, N. Bao, C. Wan, N. H. Park, K. Koumoto, and A. Gupta, *J. Power Sources*241, 255 (2013).

20. L.D. Landau, E.M. Lifshitz. *Electrodynamics of continuous media*, 2nd edn. (UK: Butterworth-Heinemann, 1984).

21. T. Seetawan, U. Seetawan, A. Ratchasin, S. Srichai, K. Singsoog, W. Namhongsa, C. Ruttanapun, and S. Siridejachai, *Procedia Eng*. 32, 1006 (2012).

22. A. Heghmanns, M. Beitelschmidt, S. Wilbrecht, K. Geradts, and G. Span, *Mater. Today Proc*. 2, 780 (2015).

23. G. Li, K. Zhou, Z. Song, X. Zhao, and J. Ji, *Energy Convers. Manag*. 161, 155 (2018).

24. G. Li, X. Chen, Y. Jin, and J. Ji, *Energy Procedia*142, 730 (2017).

Figure lists

Table captions

Table1 Parameters of two types of PV cells

Table 2 Parameters used in FEM model

Table 3 Details with the area ratio of n/p TE elements

Nomenclature

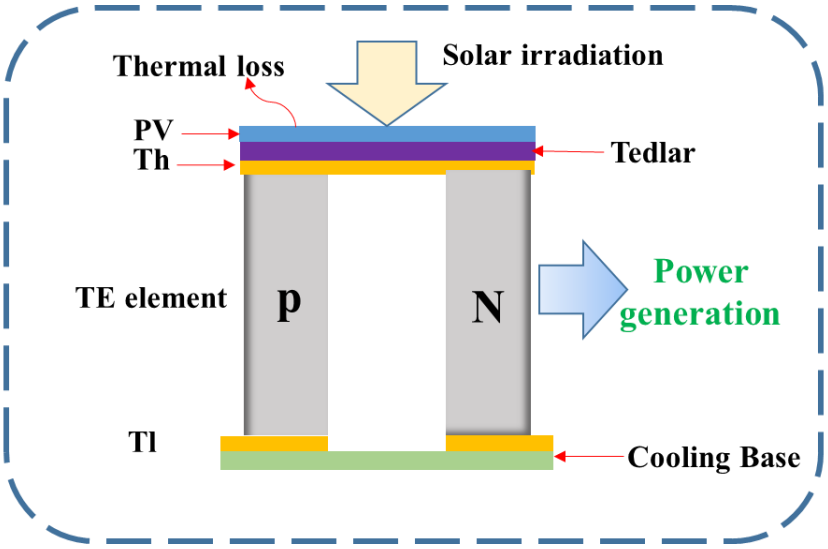

Fig. 1 Schematic diagram of a PV-TE uni-couple

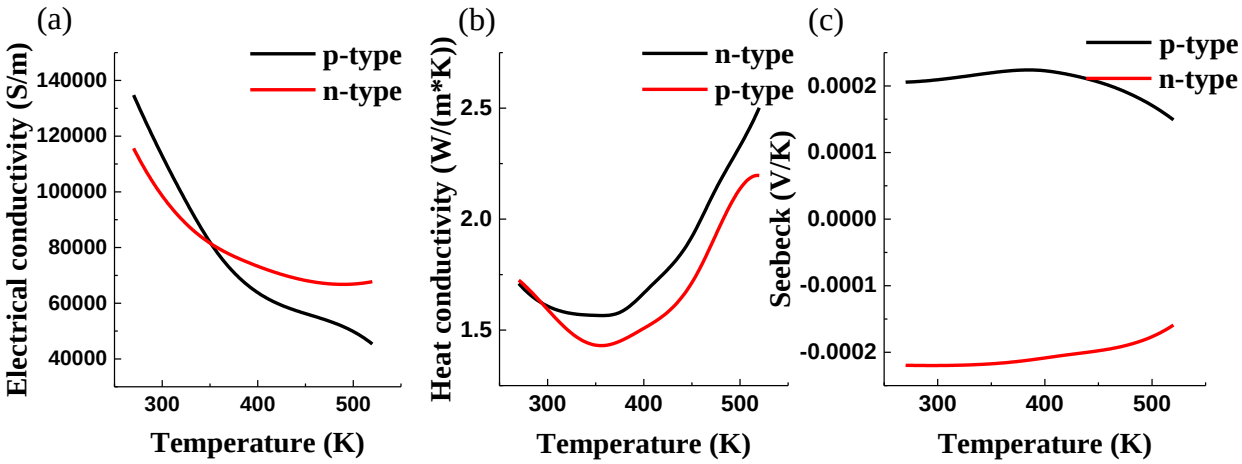

Fig. 2 Properties of the Bi_2Te_3 TE materials (a) Electrical conductivity (b) Heat conductivity (c) Seebeck

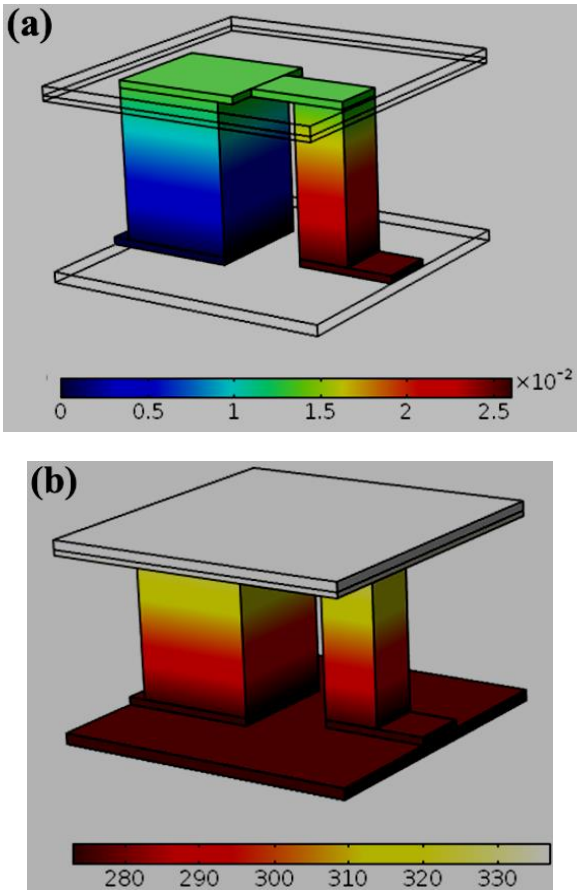

Fig. 3 Schematic diagram (a) generation of the electric voltage, (b) 3D temperature distribution of the PV-TE using PV cell Cell_1, $A_n/A_p = 4.18$, $h = 5mm$, $A_n + A_p = 18mm^2$.

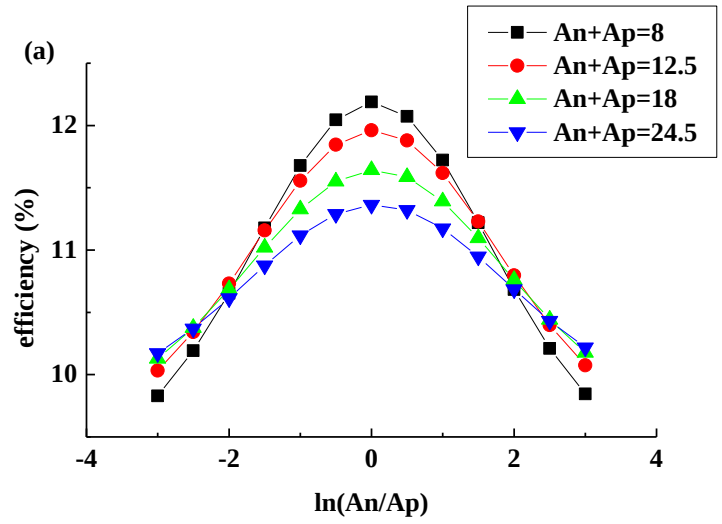
(a)
An+Ap=8
An+Ap=12.5
An+Ap=18
An+Ap=24.5
efficiency (%)
ln(An/Ap)

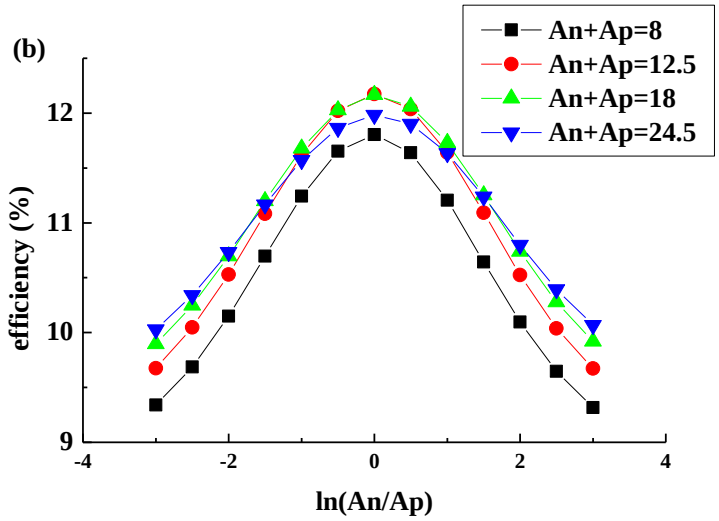
(b)
An+Ap=8
An+Ap=12.5
An+Ap=18
An+Ap=24.5
efficiency (%)
ln(An/Ap)

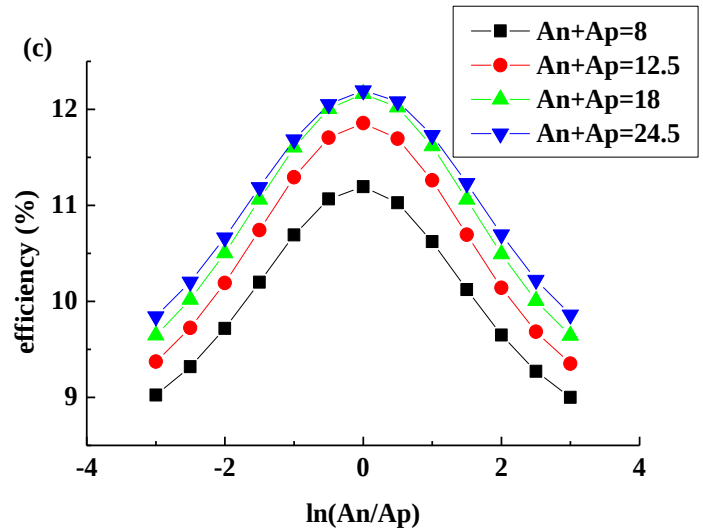
(c)
An+Ap=8
An+Ap=12.5
An+Ap=18
An+Ap=24.5
efficiency (%)
ln(An/Ap)

Fig. 4 Variation of the PV/TE efficiency with the area ratio between n-type and p-type using the PV cell Cell_1. The length of TE elements is (a) 5mm, (b) 10mm, (c) 15mm

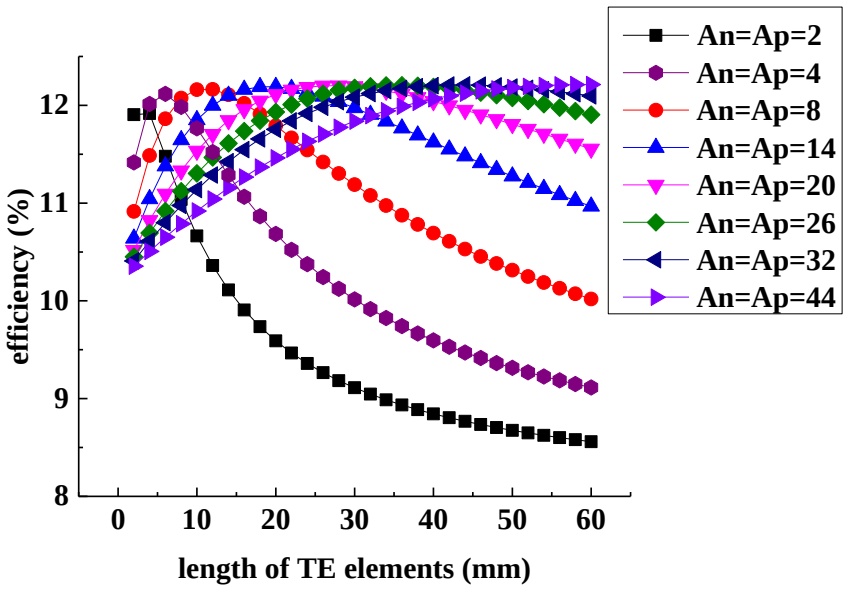

Fig. 5 Variation of the PV-TE efficiency with different length of TE elements based on Cell_1

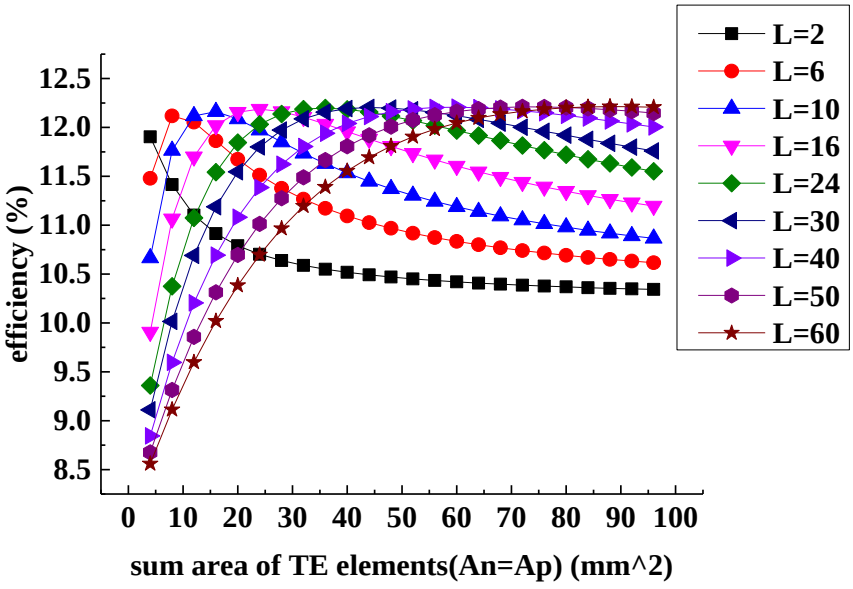

Fig. 6 Variation of the PV-TE efficiency with different footprint areas of TE elements based on Cell_1

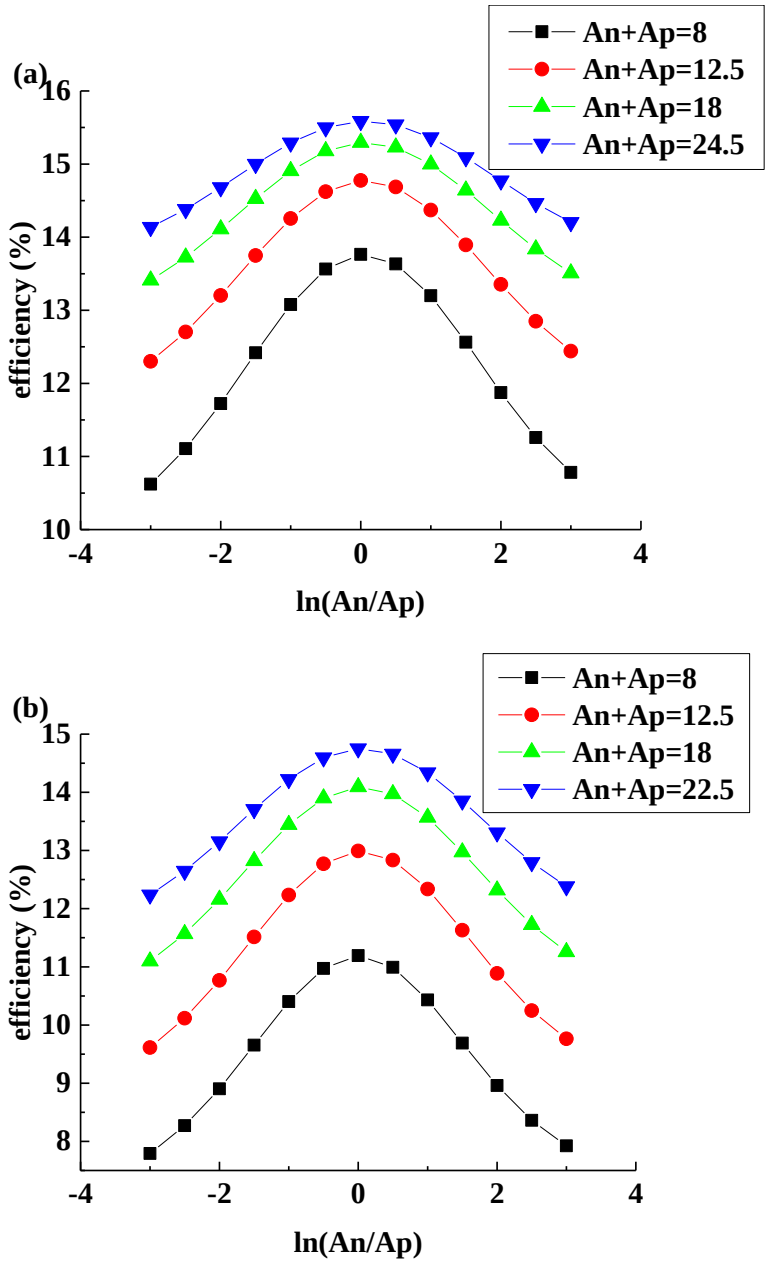

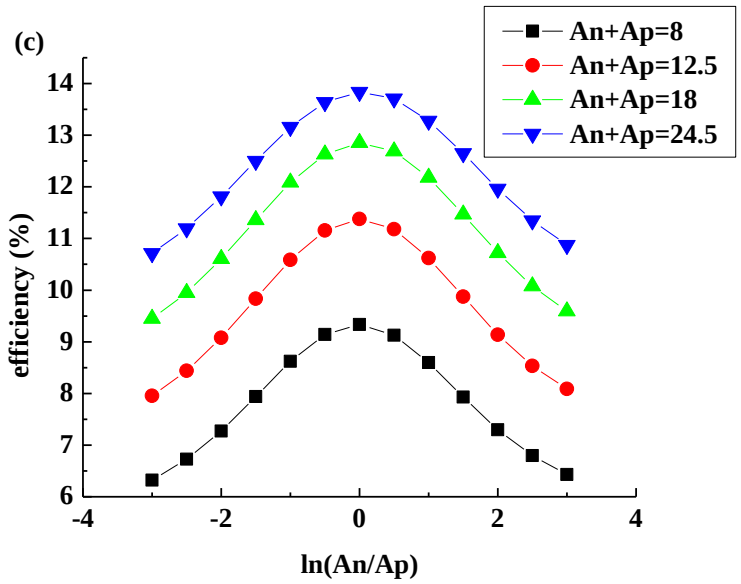

Fig. 7 Variation of the PV/TE efficiency with the area ratio between n-type and p-type using the PV cell Cell_2. The length of TE elements is (a) 5mm, (b) 10mm, (c) 15mm.

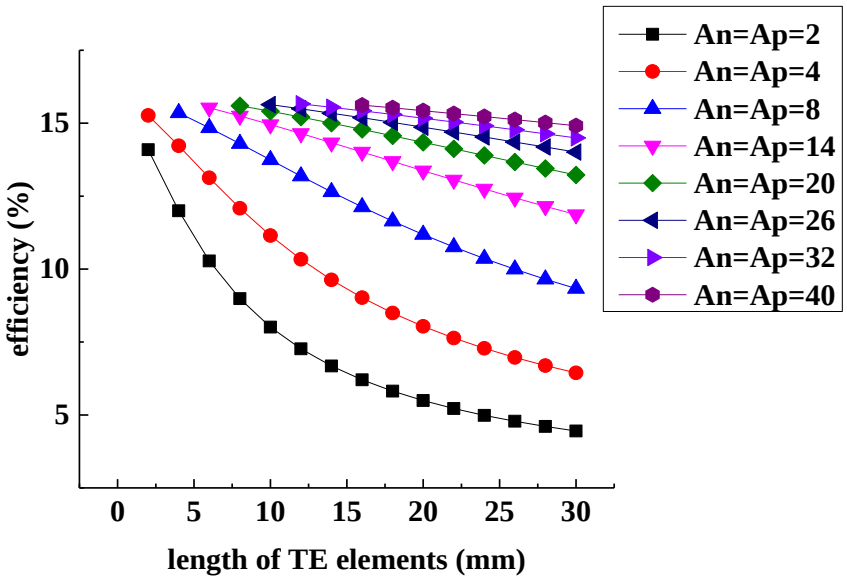

Fig. 8 Variation of the PV-TE efficiency with different length of TE elements based on Cell_2

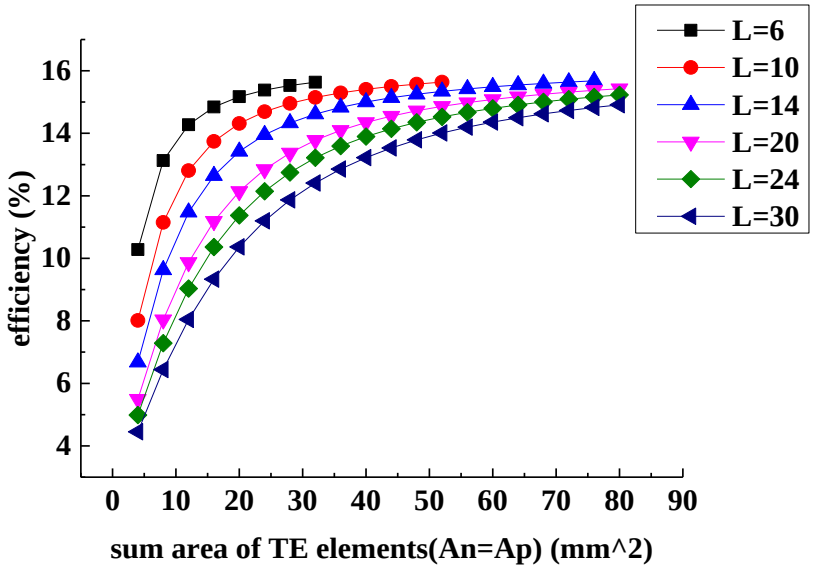

Fig. 9 Variation of the PV-TE efficiency with different footprint areas of TE elements based on Cell_2

Table 1 Parameters used in FEM model

Parameters	Symbol	Value
Area of PV cell	A_c	$10mm \times 10mm$
Thickness of PV cell	H_c	$0.3mm$
Thickness of Tedlar	H_{ted}	$0.175mm$
Thickness of metal sheet	H_{cu}	$0.1mm$
Absorptivity of PV	α_c	0.9
Thermal conductivity of PV	k_c	$148W/(m{\cdot}K)$
Thermal conductivity of tedlar	k_{ted}	$0.2W/(m{\cdot}K)$
Thermal conductivity of metal copper	k_{cu}	$401W/(m{\cdot}K)$
Emissivity of PV	ε	0.8
Ambient temperature	T_{amb}	$298K$
Wind velocity	u_w	$1m/s$
Electrical conductivity of metal copper	μ_{cu}	$58.1\times10^6 S/m$
Solar radiation	G	$1000W/m^2$
Concentration ratio	C	5

Table 2 Two types of PV cells used in the study

PV cells	Efficiency at standard condition	Temperature coefficient
Cell_1	10%	$-0.001K^{-1}$
Cell_2	15%	$-0.004K^{-1}$

Table 3 Footprint dimensions of the TE elements with the area ratio of n/p TEG elements

Design NO.	01	02	03	04	05	06	07
A_n / A_p	0.050	0.082	0.135	0.223	0.368	0.607	1.000
Design NO.	08	09	10	11	12	13	
A_n / A_p	1.649	2.718	4.482	7.389	12.182	20.086	

Nomenclature

A_c area of the solar cell (m^2)

A_n area of the n-type of TE element (m^2)

A_p area of the p-type of TE element (m^2)

C concentration ratio

C_p heat capacity at 1 atmosphere ($J \cdot kg^{-1} \cdot K^{-1}$)

E_{PV} power output of the PV cell per square meter($W \cdot m^{-2}$)

G solar irradiance ($W \cdot m^{-2}$)

h convection heat transfer coefficient ($W \cdot m^{-2} \cdot K^{-1}$)

k thermal conductivity ($W \cdot m^{-1} \cdot K^{-1}$)

l_n length of the n-type of TE element (m)

l_p length of the p-type of TE element (m)

P power output of the PV/TE system (W)

P_{PV} electricity generated by PV cell (W)

P_{TE} electricity generated by TEG (W)

T temperature (K)

T_{amb} temperature of the ambient (K)

u_{wind} wind velocity ($m \cdot s^{-1}$)

Greek symbols

α_c absorptivity of PV cell

φ solar cell temperature coefficient(K^{-1})

ρ density ($kg \cdot m^{-3}$)

η efficiency of the PV/TE system

η_c efficiency of the solar cell at standard condition

ε emissivity

σ_b Stefan-Boltzmann's constant ($= 5.67 \times 10^{-8} W \cdot m^{-2} \cdot K^{-4}$)